RESEARCH ARTICLE

Virtual Vector-Based FCS-MPC for NPC Three-Level Grid-Tied Inverter Without Weighting Factor of Neutral-Point Voltage Balancing

NAN JIN[ID], DONGREN DAI, HUAN XIE, JIE WU[ID], AND LEILEI GUO[ID]
College of Electrical and Information Engineering, Zhengzhou University of Light Industry, Zhengzhou, Henan 450002, China

Corresponding author: Jie Wu (wujie@zzuli.edu.cn)

ABSTRACT The neutral-point clamped (NPC) inverter is widely used in energy conversion, but the unbalance of neutral-point voltage (NPV) will lead to imprecise control and the decline of power quality. Conventional finite control set model predictive control (FCS-MPC) uses an extra NPV weighing factor to balance the NPV. But the weighting factor should tune frequently to match the best value. To cope with this problem, this paper proposes a virtual vector-based control strategy without the NPV weighting factor for NPC inverters. The paper analyses the relationship between neutral-point current and neutral-point voltage. An NPV vector is designed to inject a compensatory neutral-point current to balance the capacitor voltage. The duration time of each NPV vector is calculated from the real-time unbalance of the NPV. Because each NPV balancing virtual vector contains one NPV vector, the proposed method can balance the NPV without an extra NPV weighting factor in the cost function. Besides, a cost function without the NPV weighting factor is designed for the proposed method. Finally, experiments are carried out to verify the validity of the proposed method.

INDEX TERMS Model predictive control, virtual vectors, neutral-point voltage, NPC inverters, weighting factor.

I. INTRODUCTION

In recent years, with the fast development of renewable energy, Neutral-Point Clamped (NPC) three-level inverters have attracted much attention because of their superior performance in harmonics, higher operation voltage, less power loss, and lower switching stress [1], [2]. Neutral-Point voltage (NPV) balancing is essential in designing control strategies for NPC inverters [3], [4].

NPC three-level inverters have two series capacitors in DC-Link. These two capacitors are clamped by DC-Link

The associate editor coordinating the review of this manuscript and approving it for publication was Nagesh Prabhu[ID].

bus voltage, the ideal capacitance and capacitor voltage in three-level NPC inverters are designed equal. However, due to the unavoidable charge and discharge of capacitors, NPV is variable. The unbalance of NPV will result in the distortion of the output current and may be harmful to the switching devices [5]–[7]. Therefore, it is necessary to study the NPV effect of NPC three-level inverters.

Finite control set model predictive control (FCS-MPC) has attracted much attention because of its adaptability to nonlinearities, constraints, and other complex requirements [8], [9]. The fast development of digital signal processors (DSP) also reduces the calculation delay of FCS-MPC, improves the control performance, and makes control more precise.

Compared with MPC in two-level inverters, NPC three-level inverters have 27 basic vectors [10], this means more choices and accurate control.

But NPV control is still a key point in FCS-MPC. To balance NPV, an extra weighting factor is used in the cost function [11]–[13]. This conventional way must tune the weighting factor frequently due to the varying working condition. Therefore, the weighting factor must be considered while designing control strategies in conventional FCS-MPC.

To avoid the tuning of the NPV weighting factor, a weighting factor-less model predictive control method was proposed in [14]. An offset voltage was injected into the reference voltage according to the difference between the upper and lower capacitor voltages. This can balance the NPV in small oscillations. However, the reference voltage was calculated directly from the reference current, which represents the ideal output of the inverter. The adjustment of the reference voltage may change the current tracking features.

The effect to the NPV of each space voltage vector was analyzed and the vectors were categorized for vector selection in [15]. This method can naturally balance the NPV and reduce the computation time. However, only basic space voltage vectors are used. This may reduce the control effect, compared to the double-vectors.

As the double-vector strategy was widely studied [8], [16]–[18], according to the influences on NPV of double-vectors, a weighing factor-less model predictive control was proposed [19]. The method can balance the NPV without the weighting factor. However, the switching time of double-vectors was determined by the existing cost function values. This may not fully consider the switching time of NPV balancing. Besides, the dc-link capacitor voltage unbalance can be regulated using the duty cycle ratio of positive and negative short vectors [20].

This paper proposes a virtual vector-based FCS-MPC strategy without NPV weighting factor for NPC grid-tied inverters. The proposed method uses the virtual vectors to realize the weighting factor-less MPC strategy. Compared to [14], no reference voltage adjustment is used. Instead of using only basic space voltage vectors in [15], the proposed method uses the virtual vector to improve the control effect. The proposed method uses the real-time unbalance value of the NPV to calculate virtual vectors, the disadvantage of double-vectors in [19] is avoided. Except for only the utilization of short vectors in [20], middle vectors are also considered to balance the NPV. The contributions of this article are:

1. A compensatory neutral-point current injection method is proposed. The paper analyses the relationship between neutral-point current and neutral-point voltage. A compensatory neutral-point current can be injected to balance the NPV. Short vectors and middle vectors are analyzed and selected to provide this neutral-point current. Besides, a vector selection method is designed to select the short vectors or middle vectors quickly.

2. The virtual vectors with the NPV balancing ability are designed in this paper. The virtual vector is calculated from
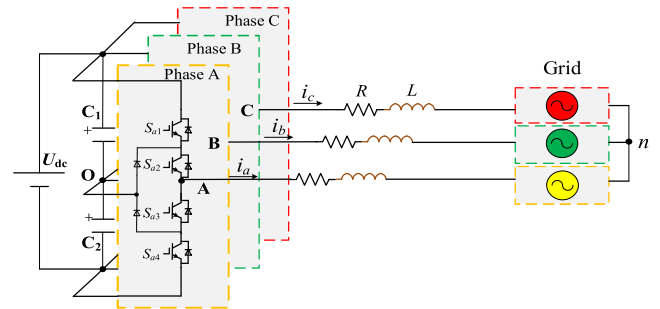

FIGURE 1. Topology of NPC three-level grid-tied inverter.

the real-time unbalance of the NPV. Each virtual vector is calculated from the neutral-point current and the unbalance of NPV. This calculation method can enhance the NPV balance ability. After selecting one virtual vector, the comparison values can be decided quickly based on the comparison value look-up table.

3. A cost function without the NPV weighting factor is designed to track the reference values. This cost function has the positive gradient, tracking the reference value with minimum space distance. Besides, this cost function is expressed with the reference voltage and the predictive voltage, which eliminates the predictive current calculation of MPC.

This paper is organized as follows. Section II introduces the topology of NPC three-level inverters, space voltage vectors, and conventional FCS-MPC for three-level inverters. In section III, to eliminate the NPV weighting factor in the cost function, the relationship between the NPV and the neutral-point current is analyzed. Then, the proposed method is presented with NPV weighing factor-less cost function. Finally, an experiment is conducted to verify the validity of the proposed method. And the conclusion is provided in Section V.

II. ANALYSIS OF NEUTRAL-POINT VOLTAGE AND CONVENTIONAL FCS-MPC

A. VOLTAGE VECTORS OF NPC INVERTER

Fig.1 shows the topology of the NPC three-phase grid-tied inverter. U_{dc} is the DC-link voltage; C_1, C_2 are DC-link capacitors; R, L, is the equivalent resistance, filter inductance, respectively. The inverter produces three voltage levels $\{-U_{dc}/2, 0, U_{dc}/2\}$. If the upper two switches S_{a1} and S_{a2} are conducted, phase A generates $U_{dc}/2$. If the lower two switches S_{a3} and S_{a4} are conducted, phase A generates $-U_{dc}/2$. If the middle two switches S_{a2} and S_{a3} are conducted, the voltage of phase A becomes zero.

Each phase has 3 switching states, the three-phase inverter can compose 27 space voltage vectors in the $\alpha\beta$ stationary stational system, as shown in Fig. 2. Generally, space voltage vectors are classified into four types according to the length of different vectors:

1) zero vectors (U_0-U_2): length is 0.
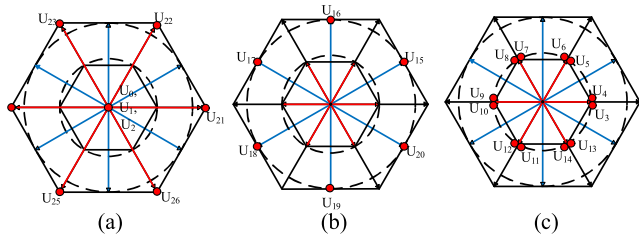2) short vectors (U_3-U_{14}): length is $U_{dc}/3$.

FIGURE 2. Categories of the vectors. (a) Long and zero vectors. (b) Middle vectors. (c) Short vectors.

3) middle vectors(U_{15}-U_{20}): length is $U_{dc}/\sqrt{3}$.
4) long vectors (U_{21}-U_{26}): length is $2U_{dc}/3$.

Defining the zero-switching function Z_x represents a phase current flowing through the neutral point. According to the Kirchhoff's circuit laws, three-phase currents flow through the neutral point as given by:

$$I_o = Z_a \times I_a + Z_b \times I_b + Z_c \times I_c$$

$$Z_x = \begin{cases} 1 & \text{phase } x \text{ connects to NP} \\ 0 & \text{other cases} \end{cases} \quad (1)$$

where I_a, I_b, and I_c are the phase current of phases a, b, and c.

Based on the above analysis, only short and middle vectors can affect the NPV because currents flow through the neutral point, leading to asynchronous discharging and charging of the capacitors. The long vectors do not connect any phase to NP, the zero vectors connect output terminals A, B, and C together. Therefore, long vectors and zero vectors do not influence capacitor voltage. Moreover, Table 1 classify all basic vectors into zero vectors, long vectors, middle vectors, and short vectors. Each type of space voltage vector can affect different capacitor voltage.

TABLE 1. Affected capacitor voltage with space voltage vector.

Vector category	Vectors	Affected capacitor voltage
Zero vectors	$U_0(0,0,0)$, $U_1(1,1,1)$, $U_2(-1,-1,-1)$	None
Long Vectors	$U_{21}(1,-1,-1)$, $U_{22}(1,1,-1)$, $U_{23}(-1,1,-1)$ $U_{24}(-1,1,1)$, $U_{25}(-1,-1,1)$, $U_{26}(1,-1,1)$	None
Middle Vectors	$U_{15}(1,0,-1)$, $U_{16}(0,1,-1)$, $U_{17}(-1,1,0)$, $U_{18}(-1,0,1)$, $U_{19}(0,-1,1)$, $U_{20}(1,-1,0)$	U_{C1} and U_{C2}
Short Vectors	$U_3(1,0,0)$, $U_5(1,1,0)$, $U_7(0,1,0)$, $U_9(0,1,1)$, $U_{11}(0,0,1)$, $U_{13}(1,0,1)$	U_{C1}
	$U_4(0,-1,-1)$, $U_6(0,0,-1)$, $U_8(-1,0,-1)$, $U_{10}(-1,0,0)$, $U_{12}(-1,-1,0)$, $U_{14}(0,-1,0)$	U_{C2}

B. CONVENTIONAL FCS-MPC STRATEGY

Fig. 3 gives the conventional MPC strategy. Grid voltage e_a, e_b, e_c, grid-tied currents I_a, I_b, I_c, and the NPV U_{np} are collected by sensors. A three-phase phase lock loop (PLL) calculates the grid voltage phase θ. After coordinate transformation, grid voltage e_α, e_β, reference currents $I_{ref\alpha}$, $I_{ref\beta}$, grid-tied currents I_α, I_β and the NPV U_{np} are used in the FCS-MPC program.
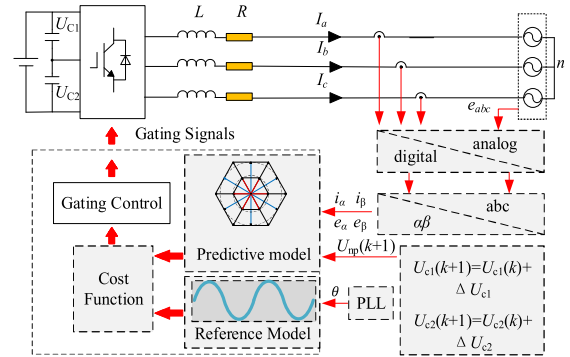

FIGURE 3. Conventional MPC with NPV weighting factor.

According to Kirchhoff Voltage Law, the inverter output voltage can be defined as:

$$\begin{bmatrix} u_{aN} \\ u_{bN} \\ u_{cN} \end{bmatrix} = R \begin{bmatrix} i_a \\ i_b \\ i_c \end{bmatrix} + L\frac{d}{dt}\begin{bmatrix} i_a \\ i_b \\ i_c \end{bmatrix} + \begin{bmatrix} e_a \\ e_b \\ e_c \end{bmatrix} \quad (2)$$

To simplify the model, Clark transformation is applied in equation (2):

$$\begin{bmatrix} u_\alpha \\ u_\beta \end{bmatrix} = R \begin{bmatrix} i_\alpha \\ i_\beta \end{bmatrix} + L\frac{d}{dt}\begin{bmatrix} i_\alpha \\ i_\beta \end{bmatrix} + \begin{bmatrix} e_\alpha \\ e_\beta \end{bmatrix} \quad (3)$$

If the sampling period T_s is short enough, equation (3) can be discretized. And the equivalent transformation, the forward-Euler approximation is used. Predictive current is obtained as:

$$\begin{bmatrix} i_\alpha(k+1) \\ i_\beta(k+1) \end{bmatrix} = (1 - \frac{RT_s}{L})\begin{bmatrix} i_\alpha(k) \\ i_\beta(k) \end{bmatrix} + \frac{T_s}{L}\begin{bmatrix} u_\alpha(k) - e_\alpha(k) \\ u_\beta(k) - e_\beta(k) \end{bmatrix} \quad (4)$$

where $u(k)$ is the applied vector. $i_x(k+1)$, $i_x(k)$ $(x = \alpha, \beta)$ are predictive and real-time grid current respectively.

The main idea of MPC is to predict the currents of $k+1$ time, and make the prediction value approach the reference currents. Therefore, the cost function in stationary coordinate is given as:

$$J_1 = (i_\alpha(k+1) - i_\alpha^*)^2 + (i_\beta(k+1) - i_\beta^*)^2 \quad (5)$$

where $i_x(k+1)$, i_x^* $(x = \alpha, \beta)$ are predictive and reference values, respectively.

When computing the cost function, the U_{c1} and U_{c2} are assumed equal to $U_{dc}/2$. Therefore, the unbalanced NPV may result in inaccurate predictions. Conventional FCS-MPC uses equation (6) with a weighting factor λ to control the NPV:

$$J_2 = \lambda|U_{np}(k+1)| \quad (6)$$

Thus, the cost function is the sum of equations (5) and (6):

$$J_3 = J_1 + J_2 \quad (7)$$

From the above analysis, conventional MPC uses an extra weighting factor in the cost function to balance NPV. Because the weighting λ can directly influence the cost function value. The tuning of the NPV weighting factor is the key point for cost function designing. An inappropriate NPV weighting factor could significantly decrease the control effect.

III. PROPOSED VIRTUAL VECTOR WITHOUT NPV WEIGHTING FACTOR IN COST FUNCTION

To eliminate NPV oscillation and simplify the cost function, a virtual vector-based FCS-MPC method without the NPV weighting factor is proposed. For each vector, its NPV effect is predictable. Therefore, it is possible to control the NPV precisely. By injecting a specific NPV vector into each control period, two vectors can be implemented in one period. Because in each switching period an NPV balancing vector can be implemented once. Thus, the NPV weighting factor is not needed.

A. VIRTUAL VECTORS SELECTION PRINCIPLE

The circuit of an NPC inverter involving the DC-link stage has shown in Fig. 1. The NPV U_{np} can be calculated from U_{c1} and U_{c2}:

$$U_{np} = \frac{1}{2}(U_{c2} - U_{c1}) \qquad (8)$$

where U_{c1} and U_{c2} represent the voltages over the upper and lower dc-link capacitors, respectively.

The relationship between capacitor voltage and current is:

$$C\frac{dU_c}{dt} = i_c \qquad (9)$$

Generally, in each sampling period T_s, the NPV will be affected by the applied switches. The NPV is a function of the neutral-point current i_o. When short vectors are selected, only one capacitor is active:

$$\begin{cases} \dfrac{C\Delta U_{c1}}{T_s} = i_o & \text{if } U_{c1} \text{ is active} \\ \dfrac{C\Delta U_{c2}}{T_s} = -i_o & \text{if } U_{c2} \text{ is active} \end{cases} \qquad (10)$$

When middle vectors are selected:

$$\frac{C(\Delta U_{c1} - \Delta U_{c2})}{T_s} = i_o \qquad (11)$$

The neutral-point current decides the NPV variation in each control period. On the contrary, to eliminate the voltage difference between C_1 and C_2, a compensation neutral-point current is deployed. This compensation neutral-point current is given by the NPV vector.

The redundant switching states such as switching state [1 0 0] and switching state [0 −1 −1] have the same current effect. Because they are in the same position on the space voltage vector diagram. But they have the opposite NPV effect, as Fig. 4 shows. Assuming $i_a > 0$, Fig. 4 shows the impact on NPV of these two redundant switching states. The selection of switching state [1 0 0] would charge the C_1, and U_{c1} would increase, resulting in the decrement of U_{np}. Otherwise, if the switching state [0 −1 −1] is selected, U_{c2} increases, resulting in the increment of U_{np}. Other pairs of short vectors can be analyzed in the same way.

Therefore, benefiting from the redundant short vectors, a NPV vector can be selected without changing the position on the space voltage vector diagram. Due to
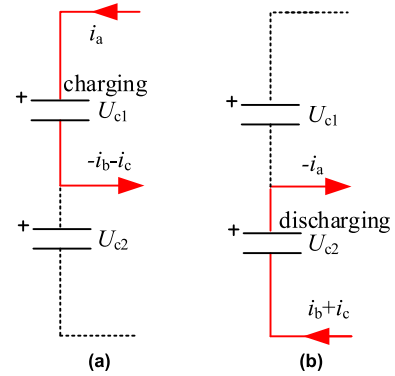

FIGURE 4. The impact on NPV of two redundant switching states. (a) Switching state [1 1 0]. (b) Switching state [0 −1 −1].
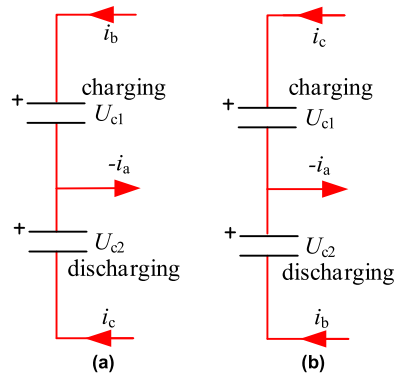

FIGURE 5. The impact on NPV of switching states [0 1 −1] and [0 −1 1]. (a) Switching state [0 1 −1]. (b) Switching state [0 −1 1].

$i_a + i_b + i_c = 0$, there is always an available compensatory neutral-point current to compensate for the unbalance of NPV.

Fig. 5 shows when phase A connects to the neutral point, the impact on NPV of switching states [0 1 −1] and [0 −1 1]. Whether the switching state [0 1 −1] or [0 −1 1] is selected, the neutral-point current is $-i_a$. According to Table. 1, for middle vectors, only one phase is connected to the neutral point. Thus, the other 2 pairs of middle vectors can be proved in the same way.

To fast decide which short vectors are available, a neutral point phase selection diagram is introduced in Fig. 6. For example, when θ is π, if U_{np} is larger than zero, phase A should be connected to the neutral point. Otherwise, if U_{np} is lower than zero, phase B should be connected to the neutral point. Additionally, the NPV effect of middle vectors is only decided by which phase connects to the neutral point. Therefore, the neutral point phase can be decided by simply judging the direction of phase currents. For $U_{np} > 0$, a neutral-point current larger than zero is required. Otherwise, for $U_{np} > 0$, a neutral-point current lower than zero is required.

Fig. 7 shows the space voltage diagram when phase A connects to the neutral point. The candidate vectors are 6 short vectors, 2 middle vectors, and 1 zero vector, corresponding to 9 switching combinations of the remaining two phases. These vectors are divided into 6 sectors. According to the sector
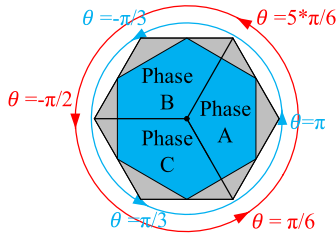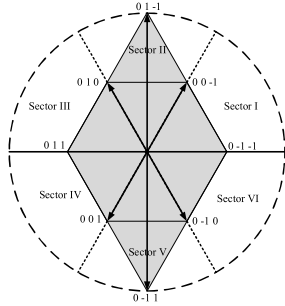
FIGURE 6. Neutral-point phase selection diagram.

FIGURE 7. Space voltage vector diagram when phase A connects to the neutral point.

FIGURE 8. Synthesis strategy for virtual vectors.
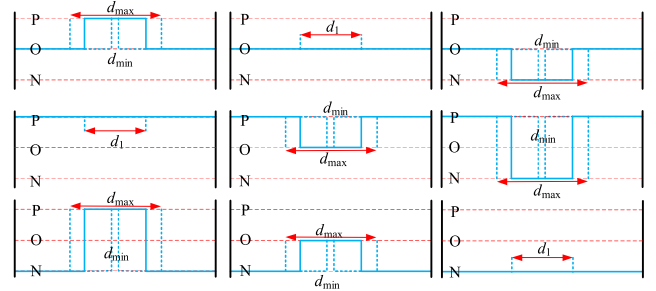
FIGURE 9. NPV vector injection strategy.

division strategy [21], [22], each sector has at least two NPV vectors, sector II and sector V has one more middle vector.

The conventional predictive model (3) and (4) may import a heavy computational burden for implementation. And the NPV weighing factor is not needed in the proposed method. To reduce the computational burden, a cost function for the proposed method is designed.

B. IMPROVED COST FUNCTION WITHOUT NPV WEIGHTING FACTOR

Take the partial derivative of (7) with α, β:

$$\text{grand} \, (J) \, \big|_{(\alpha, \beta)} = -2 \begin{pmatrix} M_\alpha(k+1) \dfrac{\partial i_\alpha^*(k+1)}{\partial \alpha} \\ M_\beta(k+1) \dfrac{\partial i_\beta^*(k+1)}{\partial \beta} \end{pmatrix} \quad (12)$$

Equation (5) lists the predictive $k+1$ current:

$$\frac{\partial J}{\partial \alpha} = \frac{2T_s}{L} \left(\left(1 - \frac{RT_s}{L} \right) i_\alpha(k) - i_\alpha^*(k) \right.$$
$$\left. + \frac{\Delta t}{L} U_\alpha(k) - \frac{\Delta t}{L} e_\alpha(k) \right)$$
$$\frac{\partial J}{\partial \beta} = \frac{2T_s}{L} \left(\left(1 - \frac{RT_s}{L} \right) i_\beta(k) - i_\beta^*(k) \right.$$
$$\left. + \frac{\Delta t}{L} U_\beta(k) - \frac{\Delta t}{L} e_\beta(k) \right) \quad (13)$$

Second derivative (13):

$$\frac{\partial J}{\partial \alpha} = 2 \left(\frac{T_s}{L} \right)^2 > 0$$
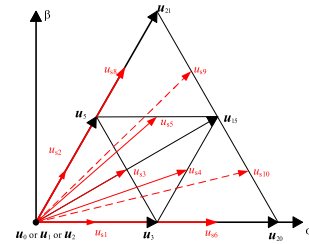$$\frac{\partial J}{\partial \beta} = 2 \left(\frac{T_s}{L} \right)^2 > 0 \quad (14)$$

Therefore, cost function without NPV weighting factor is given as:

$$J_4 = \left(\frac{T_s}{L} \right)^2 \left[U_\alpha^{opt} - u_\alpha \quad U_\beta^{opt} - u_\beta \right] \begin{bmatrix} U_\alpha^{opt} - u_\alpha \\ U_\beta^{opt} - u_\beta \end{bmatrix} \quad (15)$$

where U^{opt} is the space voltage vector which can minimalize the cost function.

According to equations (5) and (6), the ideal situation is $i(k+1)$ equals to $i^*(k)$. Therefore, replace $i(k+1)$ with $i^*(k)$:

$$I_\alpha(k+1) = \frac{T_s}{L} U_\alpha^{opt} + \left(1 - \frac{RT_s}{L} \right) I_\alpha(k) - \frac{T_s}{L} e_\alpha(k)$$
$$I_\beta(k+1) = \frac{T_s}{L} U_\beta^{opt} + \left(1 - \frac{RT_s}{L} \right) I_\beta(k) - \frac{T_s}{L} e_\beta(k) \quad (16)$$

The optimal space voltage vector with minimum space distance is expressed as:

$$U_\alpha^{opt} = \frac{L}{T_s} I_\alpha^* - \left(\frac{L}{T_s} - R \right) I_\alpha(k) + e_\alpha(k)$$
$$U_\beta^{opt} = \frac{L}{T} I_\beta^* - \left(\frac{L}{T_s} - R \right) I_\beta(k) + e_\beta(k) \quad (17)$$

C. NPV BALANCING VIRTUAL VECTOR SYNTHESIS AND IMPLEMENTATION

Fig. 8 shows the virtual vector synthesis results of Sector I. For virtual vectors u_{s1} to u_{s8}, one NPV vector can participate in the synthesis procedure. For virtual vectors u_{s9} and u_{s10}, it is dependent on whether the middle vector u_{15} is included in the NPV vectors. If it is, the virtual vectors u_{s9} and u_{s10} are available. Otherwise, these two virtual vectors are not available, u_{20} and u_{21} are alternative vectors.

Fig. 9 shows the examples of NPV vector injection strategies. The proposed method inserts an NPV vector into each switching period. Thus, a compensatory neutral point current
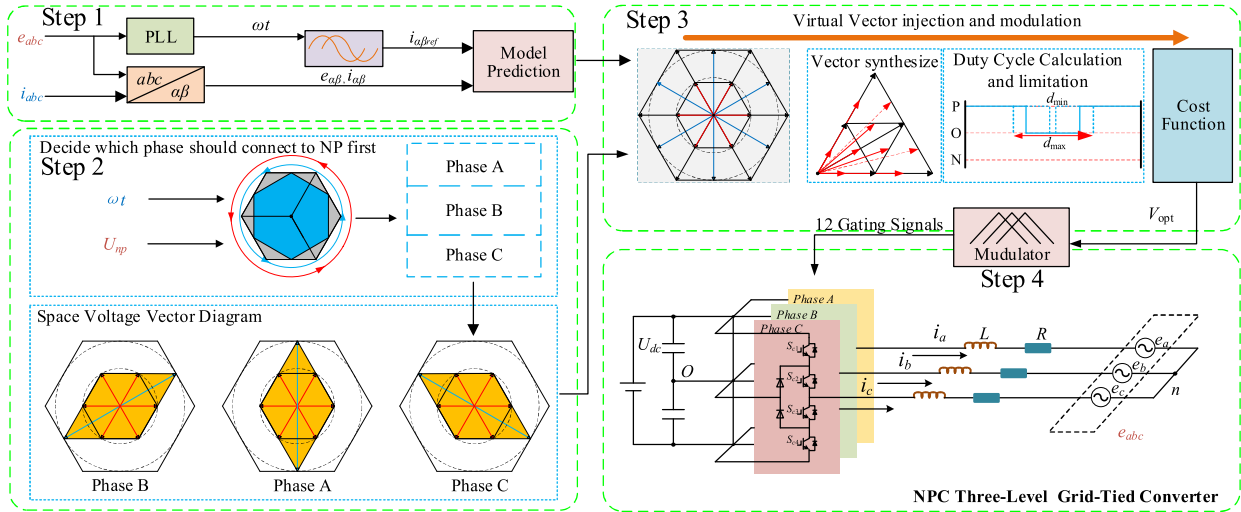
FIGURE 10. Proposed control strategy implementation flow.

TABLE 2. Comparison values for switching control.

S_{NPV}	S_{basic}	Upper value	Lower value
P	P	1	1
	N	$2d_1-1$	$2d_1-1$
	O	$2d_1-1$	1
N	P	$1-2d_1$	$1-2d_1$
	N	-1	-1
	O	-1	$1-2d_1$
O	P	$1-2d_1$	1
	N	-1	$2d_1-1$
	O	-1	1

is implemented in each switching period. In one phase, each basic vector and NPV vector has 3 switching states. Therefore, there are 9 types of injection models for each phase. The d_x (x = 1, min, max) represents the conduction time, minimum conduction time, and maximum conduction time of the NPV vector, respectively. Since the conduction time of the NPV vector is calculated by:

$$d_1 = \frac{C(U_{c1}(k) - U_{c2}(k))}{2i_o(k)} \times \frac{1}{T_s} \qquad (18)$$

There are three rules:

1) Conduction time d_1 of V_{NPV} is changeable based on the computational results.

2) d_{min} is the minimum switching interval, all the $d_1 < d_{min}$ is rounded.

3) d_{max} limits the conduction time of the NPV vector.

For implementation, the experimental controller device provides the triangular carrier wave with an amplitude of 1, the comparison values are presented in Table. 2. S_{NPV} and S_{basic} are switching state of the NPV vector and basic vector, respectively. The upper value controls the on-off of S_{x1} and S_{x3}, while the lower value controls S_{x2} and S_{x4}.

D. PROPOSED STRATEGY IMPLEMENTATION FLOW
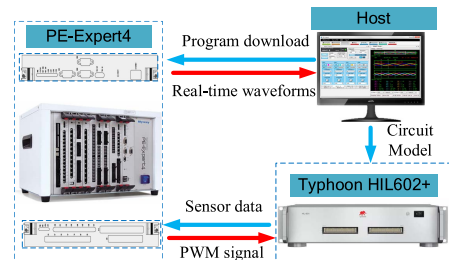Fig. 10 draws the implementation flow of the proposed method:

FIGURE 11. HIL experiment platform for the proposed plan.

Step 1: Get sensor data and make the coordinate transformation.

Step 2: Select one phase, and connect it to the neutral point. Then proper NPV vectors can be selected.

Step 3: Based on the results of virtual vector synthesizing, calculate the cost function values.

Step 4: Select the virtual vector corresponding to the minimum cost function value, then implement it based on the PWM comparison strategy.

IV. EXPERIMENT VERIFICATION
To verify the advantages and performance of the proposed algorithm, the experiment is carried out based on Typhoon HIL602+ and PE-Expert4 in Fig. 11. The HIL (Hardware in the Loop) runs a real-time circuit. The circuit model is modified in the host and loaded into Typhoon HIL602+. PE-Expert4 is a real-time controller, which runs the MPC program in the TMS320C6657 DSP core board. The controller gets necessary sensor data from the extension board, which concludes an 8-channel 14bit A/D converter. The host receives the real-time waveform from devices and sends the instructions to PE-Expert4. Experimental parameters are given in Table 3.

A. STEADY-STATE EXPERIMENT.
For the steady-state experiment, the reference currents are set to 10A. Conventional MPC with λ = 0.2, λ = 0.6,
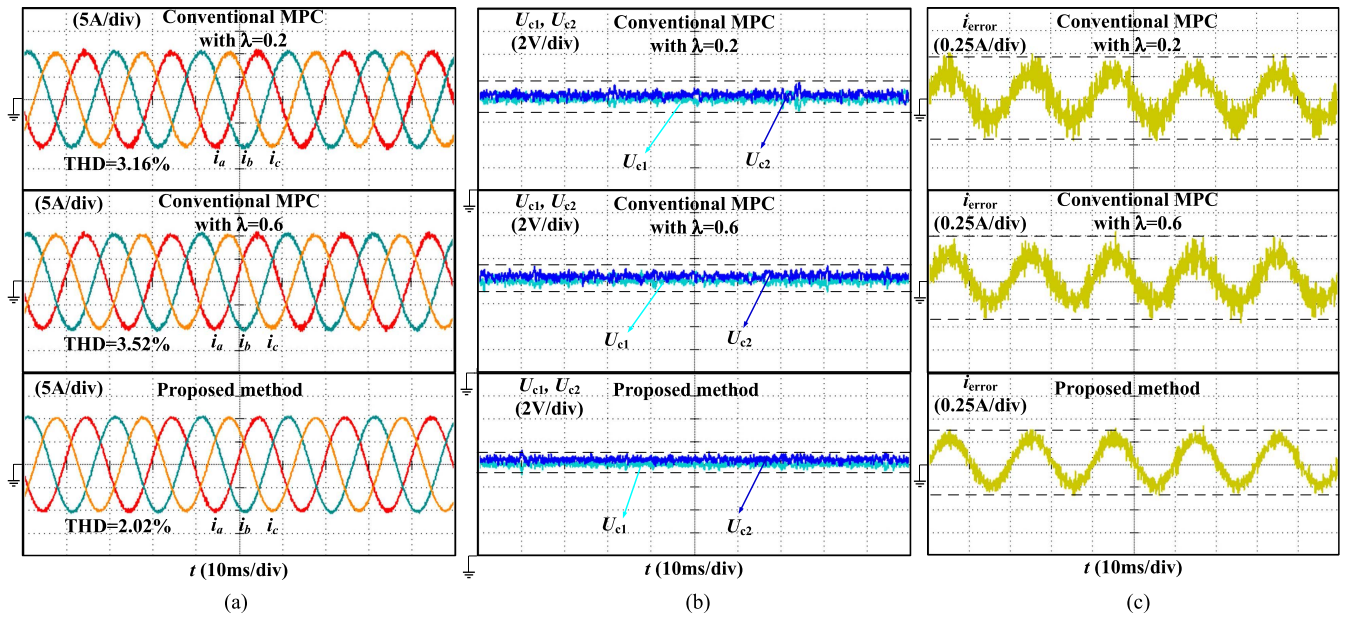
FIGURE 12. Steady-state waveforms and harmonics. (a) Output current comparisons between conventional and proposed method. (b) NPV comparisons between conventional and proposed method. (c) Current tracking error comparison.

TABLE 3. Experimental parameters.

Parameter	Description	Value
U_{dc}	DC voltage	400 V
e	Grid voltage	110 V_{rms}
R	Wire equivalent resistance	0.02 Ω
L	Filter inductance	10 mH
C_1, C_2	DC-link capacitance	1200 μF
f_s	Switching frequency	20 kHz

and the proposed method are compared. The comparisons include three dimensions: output currents comparison, NPV comparison, and current tracking error comparison.

Fig.12 shows the experiments of three methods, and Fig.13 shows the THD diagram of the experiments exceed in Fig.12. Fig.12 (a) shows the output currents comparisons of three methods. The THD of conventional strategy with $\lambda = 0.2$ is 3.16%. The THD of conventional strategy with $\lambda = 0.6$ is 3.52%, which shows a higher THD than $\lambda = 0.2$.

The THD of the proposed method without λ is 2.02%, showing better performance than the conventional strategy. Fig. 13 provides the detailed THD analysis diagrams of three methods. Fig. 12 (b) shows the U_{c1}, U_{c2} fluctuation of three methods. Higher λ results in lower NPV fluctuation. However, the output currents will distort. The proposed method can balance the NPV in lower fluctuation than the conventional method. Fig.12 (c) shows the current tracking error of three methods, proposed method has a lower peak tracking error and better lower tracking fluctuation than the conventional method.

B. DYNAMIC STATE EXPERIMENT
Fig. 14 shows the NPV rebalancing of three methods. The initial unbalance of NPV is caused by the conventional MPC with $\lambda = 0$, then switching to the testing methods. When
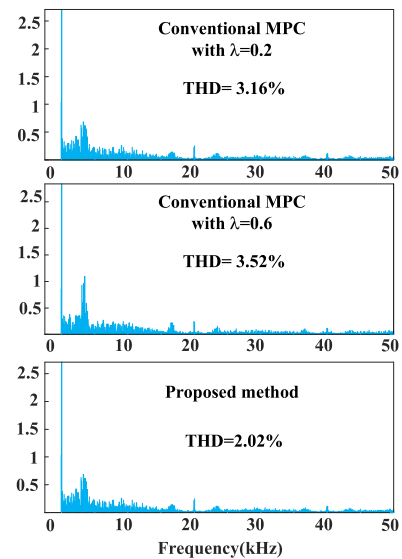

FIGURE 13. THDs of conventional MPC with $\lambda = 0.2$, $\lambda = 0.6$, and proposed method.

NPV is unbalanced, the weighting factor does not influence the rebalance. However, with the proposed method, the time of NPV rebalance is decreased from almost 0.8s to 0.6s.

Fig. 15 shows the NPV balancing and current tracking performance using conventional MPC with a finetuned weighting factor and proposed method. At begin, the reference current is 20A, both two methods can balance the NPV and trace the reference current well. After the reference current decrease to 10A, the conventional MPC with fixed weighting factor can no longer balance the NPV well. But for the proposed weighting factor-less control strategy, the NPV is stable before and after the dynamic state.
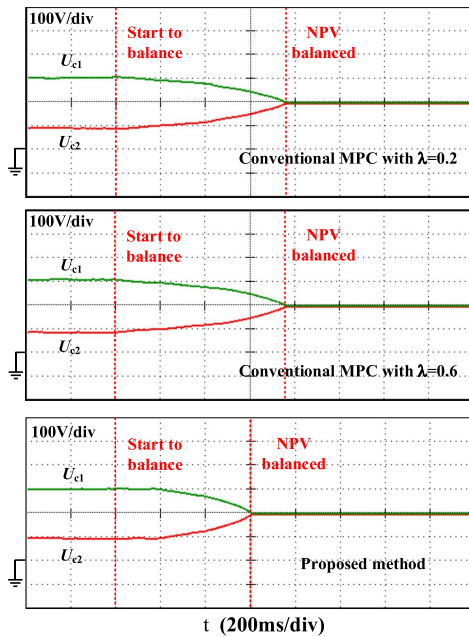
FIGURE 14. NPV rebalancing conventional MPC with λ = 0.2, λ = 0.6, and proposed method.
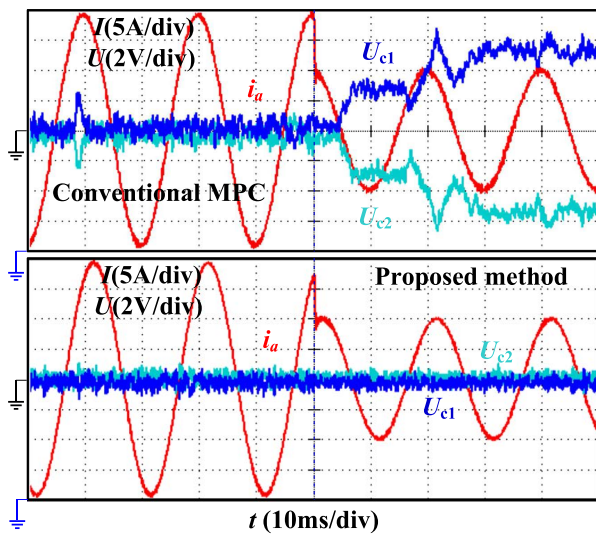

FIGURE 15. NPV balancing and current tracking performance with changing reference current.

V. CONCLUSION

In this paper, to cope with the unbalance of NPV, a virtual vector-based FCS-MPC without neutral-point voltage weighting factor is proposed. This paper analyses the relationship between neutral-point current and neutral-point voltage. A compensatory neutral-point current injection method is designed to balance the NPV. Based on this method, space voltage vectors are classified, and virtual vectors are generated. The NPV can be balanced by selecting the virtual vectors. Compared with the conventional MPC, the virtual vector scheme was adopted to track reference current precisely. Besides, a cost function without the NPV weighting factor is designed, and the sector selection is implemented

to simplify the vector selection. The proposed method is an extension of FCS-MPC, no extra sensor or hardware is introduced. The proposed method can improve the control effect of NPC three-level grid-tied inverters. Finally, experiments are conducted to verify the validity of the proposed method.

REFERENCES

[1] P. Alemi and D.-C. Lee, "Power loss comparison in two- and three-level PWM converters," in *Proc. 8th Int. Conf. Power Electron.-ECCE Asia*, May 2011, pp. 1452–1457.

[2] M. Novak, V. Ferreira, M. Andresen, T. Dragicevic, F. Blaabjerg, and M. Liserre, "FS-MPC based thermal stress balancing and reliability analysis for NPC converters," *IEEE Open J. Power Electron.*, vol. 2, pp. 124–137, 2021.

[3] C.-Q. Xiang, C. Shu, D. Han, B.-K. Mao, X. Wu, and T.-J. Yu, "Improved virtual space vector modulation for three-level neutral-point-clamped converter with feedback of neutral-point voltage," *IEEE Trans. Power Electron.*, vol. 33, no. 6, pp. 5452–5464, Jun. 2018.

[4] K. D. Pham and N. V. Nguyen, "A reduced common-mode-voltage pulsewidth modulation method with output harmonic distortion minimization for three-level neutral-point-clamped inverters," *IEEE Trans. Power Electron.*, vol. 35, no. 7, pp. 6944–6962, Jul. 2020.

[5] X. Zhou and S. Lu, "Influence of digital delay on the zero-sequence voltage injection neutral-point potential balance algorithm for three-level NPC inverters and its compensation method," *IEEE Access*, vol. 7, pp. 71593–71606, 2019.

[6] X. Xing, X. Li, F. Gao, C. Qin, and C. Zhang, "Improved space vector modulation technique for neutral-point voltage oscillation and common-mode voltage reduction in three-level inverter," *IEEE Trans. Power Electron.*, vol. 34, no. 9, pp. 8697–8714, Sep. 2019.

[7] J. Rodriguez, S. Bernet, P. K. Steimer, and I. E. Lizama, "A survey on neutral-point-clamped inverters," *IEEE Trans. Ind. Electron.*, vol. 57, no. 7, pp. 2219–2230, Jul. 2010.

[8] M. Aguirre, S. Kouro, C. A. Rojas, J. Rodriguez, and J. I. Leon, "Switching frequency regulation for FCS-MPC based on a period control approach," *IEEE Trans. Ind. Electron.*, vol. 65, no. 7, pp. 5764–5773, Jul. 2018.

[9] N. Jin, M. Chen, L. Guo, Y. Li, and Y. Chen, "Double-vector model-free predictive control method for voltage source inverter with visualization analysis," *IEEE Trans. Ind. Electron.*, vol. 69, no. 10, pp. 10066–10078, Oct. 2022, doi: 10.1109/TIE.2021.3128905.

[10] F. Donoso, A. Mora, R. Cárdenas, A. Angulo, D. Sáez, and M. Rivera, "Finite-set model-predictive control strategies for a 3L-NPC inverter operating with fixed switching frequency," *IEEE Trans. Ind. Electron.*, vol. 65, no. 5, pp. 3954–3965, May 2018.

[11] C. Xue, D. Zhou, and Y. Li, "Finite-control-set model predictive control for three-level NPC inverter-fed PMSM drives with *LC* filter," *IEEE Trans. Ind. Electron.*, vol. 68, no. 12, pp. 11980–11991, Dec. 2021.

[12] A. Mora, R. Cardenas, R. P. Aguilera, A. Angulo, P. Lezana, and D. D.-C. Lu, "Predictive optimal switching sequence direct power control for grid-tied 3L-NPC converters," *IEEE Trans. Ind. Electron.*, vol. 68, no. 9, pp. 8561–8571, Sep. 2021.

[13] T. Jin, Y. Huang, Y. Lin, and M.-N. D. Legrand, "Model predictive current control based on virtual voltage vector method for parallel three-level inverters," *IEEE J. Emerg. Sel. Topics Power Electron.*, vol. 9, no. 5, pp. 6049–6058, Oct. 2021.

[14] E.-S. Jun, M. H. Nguyen, and S.-S. Kwak, "Model predictive control method with NP voltage balance by offset voltage injection for three-phase three-level NPC inverter," *IEEE Access*, vol. 8, pp. 172175–172195, 2020.

[15] Y. Yang, H. Wen, M. Fan, M. Xie, and R. Chen, "Fast finite-switching-state model predictive control method without weighting factors for T-type three-level three-phase inverters," *IEEE Trans. Ind. Informat.*, vol. 15, no. 3, pp. 1298–1310, Mar. 2019.

[16] Y. Zhang, W. Xie, Z. Li, and Y. Zhang, "Low-complexity model predictive power control: Double-vector-based approach," *IEEE Trans. Ind. Electron.*, vol. 61, no. 11, pp. 5871–5880, Nov. 2014.

[17] W. Chen, S. Zeng, G. Zhang, T. Shi, and C. Xia, "A modified double vectors model predictive torque control of permanent magnet synchronous motor," *IEEE Trans. Power Electron.*, vol. 34, no. 11, pp. 11419–11428, Nov. 2019.

[18] X. Zhang and B. Hou, "Double vectors model predictive torque control without weighting factor based on voltage tracking error," *IEEE Trans. Power Electron.*, vol. 33, no. 3, pp. 2368–2380, Mar. 2018.

[19] T. Liu, A. Chen, C. Qin, J. Chen, and X. Li, "Double vector model predictive control to reduce common-mode voltage without weighting factors for three-level inverters," *IEEE Trans. Ind. Electron.*, vol. 67, no. 10, pp. 8980–8990, Oct. 2020.

[20] D. Xiao, K. S. Alam, I. Osman, M. P. Akter, S. M. S. I. Shakib, and M. F. Rahman, "Low complexity model predictive flux control for three-level neutral-point clamped inverter-fed induction motor drives without weighting factor," *IEEE Trans. Ind. Appl.*, vol. 56, no. 6, pp. 6496–6506, Nov. 2020.

[21] Y. Son and J. Kim, "A novel phase current reconstruction method for a three-level neutral point clamped inverter (NPCI) with a neutral shunt resistor," *Energies*, vol. 11, no. 10, pp. 2616–2634, Oct. 2018.

[22] W. Jiang, P. Wang, M. Ma, J. Wang, J. Li, L. Li, and K. Chen, "A novel virtual space vector modulation with reduced common-mode voltage and eliminated neutral point voltage oscillation for neutral point clamped three-level inverter," *IEEE Trans. Ind. Electron.*, vol. 67, no. 2, pp. 884–894, Feb. 2020.

NAN JIN received the B.S. and M.S. degrees in electrical engineering from the Zhengzhou University of Light Industry, Zhengzhou, China, in 2003 and 2007, respectively, and the Ph.D. degree in power electronics and electrical drives from Shanghai Jiao Tong University, Shanghai, China, in 2012. He is currently a Professor in electrical engineering with the Zhengzhou University of Light Industry. He was a Visiting Professor with the Department of Electrical Engineering and Computer Science, The University of Tennessee, Knoxville, Tennessee, USA. He has published more than 50 technical papers in journals and conference proceedings, two books, and hold 40 Chinese patents. His research interests include model predictive control method for power converter, fault diagnosis, and tolerant control of power electronics systems. He was a recipient of the 2018 Highlighted Paper Award from IEEE TRANSACTIONS ON POWER ELECTRONICS.

DONGREN DAI was born in Henan, China, in 1996. He received the B.S. degree in building electricity and intelligence from the Zhengzhou University of Light Industry, Zhengzhou, China, in 2019, where he is currently pursuing the master's degree. His research interest includes model predictive control for power converters.

HUAN XIE was born in Shandong, China. He received the B.S. degree in electrical engineering from the Changchun Institute of Technology, China, in 2020. He is currently pursuing the M.S. degree with the Zhengzhou University of Light Industry. His research interest includes model predictive control for power converters.

JIE WU received the M.Eng. degree in electrical engineering from the Hubei University of Technology, Wuhan, China, in 2005, and the Ph.D. degree from the VŠB-Technical University of Ostrava, Czech Republic, in 2012. He is currently an Associate Professor with the Zhengzhou University of Light Industry, Zhengzhou, China. He has authored or coauthored more than 60 refereed journal/conference papers or books. He contributed to the AC flux control technology in hybrid excitation machine. His research interests include electrical power engineering, such as simultaneous wireless information and power transfer, power electronic drives, and electrical machines.

LEILEI GUO was born in Henan, China, in 1987. He received the B.S. and Ph.D. degrees in electrical engineering from the School of Electrical Engineering and Automation, Hefei University of Technology, Hefei, China, in 2010 and 2016, respectively. He is currently an Associate Professor in electrical engineering with the Zhengzhou University of Light Industry. He was selected into the Young Talent Promotion Plan of Henan Province, in 2018. He has published more than 30 technical papers in journals and conference proceedings. His current research interests include model predictive control of induction motors, permanent-magnet synchronous motors, and power converters.

• • •